aerospace

MDPI

Article

HCF and LCF Analysis of a Generic Full Admission Turbine Blade

Jörg R. Riccius * and Evgeny B. Zametaev

German Aerospace Center, DLR Lampoldshausen, D-74239 Hardthausen, Germany
* Correspondence: joerg.riccius@dlr.de

Abstract: A numerical turbine-blade fatigue-life analysis method is suggested. This method comprises a stationary thermal 3D finite element (FE) analysis of the hot run for the combined high-cycle fatigue (HCF) and creep analysis, and a follow-on (one-way coupled) quasi-stationary structural 3D FE analysis (including six load steps) of a single and two half turbine blades and the related disk and rotor section and a (modified Goodman equation based) post-processing fatigue life analysis for the highest HCF-loaded point of the turbine blade. For the low-cycle fatigue (LCF) analysis, this includes a transient thermal 3D FE analysis of two full loading cycles, a follow-on (one-way coupled) quasi-stationary structural 3D finite element analysis of a single and two half turbine blades and the related disk and rotor section and a (modified-Langer-equation-based) post-processing fatigue life analysis approach for the highest LCF-loaded point of the turbine blade. Finally, this approach is demonstrated by the numerical HCF, LCF and creep analysis of a generic turbine blade of the first rotor row of a full admission hydrogen turbo pump of a 1 MN thrust class gas generator LOX-LH_2 liquid rocket engine (LRE). For this numerical example, the LCF loading turned out to be dominant. Creep turned out to be negligible.

Keywords: LRE; HCF; LCF; FE; thermal analysis; structural analysis; mean stress; creep; full admission; turbine blade; post-processing; Goodman; Langer; Inconel 718

Citation: Riccius, J.R.; Zametaev, E.B. HCF and LCF Analysis of a Generic Full Admission Turbine Blade. *Aerospace* **2023**, *10*, 154. https://doi.org/10.3390/aerospace10020154

Academic Editor: Qingfei Fu

Received: 2 September 2022
Revised: 24 December 2022
Accepted: 25 December 2022
Published: 8 February 2023

1. Introduction

For high-thrust liquid rocket engines (LREs) with both high specific impulse and high thrust-to-weight ratio, propellant turbo pump(s) are essential. One of the many ingredients for obtaining a high power-to-weight ratio for a turbo pump is a large rotational speed. This results in a high tensile pre-stressing of all of the turbine blades of the rotor. Additionally, (circumferential and axial direction) flow variations of the turbine driving gas, ejected from the stator row(s) of the turbo pump, cause a severe HCF loading of all of the turbine blades. On top of this, fast start-up transients of the turbine can cause an additional LCF loading of the turbine blades. Furthermore, high turbine-driving-gas temperatures might cause turbine-blade creep.

From cracks reported at many different turbine-blade positions during the pre-development and pre-qualification phases of the well-known Space Shuttle main engine (SSME) [1] up to recently observed cracks during the pre-development phase of the fuel turbopump of the Japanese LE-5B engine [2], the list of fatigue-life-related turbine-blade problems is long. This shows the necessity of a generally applicable numerical fatigue-life analysis method—which is the main content of this paper.

The most complete historic LRE turbine-blade low-cycle fatigue-life analysis known to the authors of this paper can be found in [1], which contains, for the considered SSME turbine blade (on top of other numerical analyses):

- A 3D thermal FE analysis.
- A 3D structural FE analysis.
- A post processing (cyclic strain based) LCF analysis.

As the Coffin–Manson law used for the abovementioned LCF analysis is based on uniaxial LCF tests under high-pressure hydrogen, environmental hydrogen embrittlement (EHE) is taken into account at the same instance. Due to the huge number of HCF cycles (15 Mcycles for each full-length hot run of SSME) a catastrophic HCF failure is assumed as soon as cracks are initiated by the LCF loading. Therefore, a dedicated HCF analysis was omitted in [1]. In a more recent study [3], the classic Goodman equation is applied for the HCF analysis of a LRE turbine blade. However, in [4] it was pointed out that the classic Goodman equation is not always the best choice to take into account mean stress effects for the HCF analysis of turbine-blade materials. Turbomachinery of gas turbines is subjected to similar thermal and mechanical loading as the turbopumps of LREs. The most comprehensive turbomachinery fatigue-life related analysis known to the authors of this paper is shown in [5], which contains, e.g., effects such as LCF, HCF (including mean stress influence), creep and corrosion (oxidation and sulphidation).

The authors of this papers restrict themselves to HCF (including mean-stress and hydrogen embrittlement effects) and LCF. As fuel-rich gas drives the turbine(s) of gas-generator LREs, corrosion effects are not considered in the framework of this paper. Creep is taken into account by the FE analysis. However, as creep deformation turned out to be negligible for the loading conditions of a gas-generator-driven hydrogen turbo pump [6] of a 1 MN thrust class LRE (considered as reference turbo pump in the course of this paper), no creep term for the post-processing turbine life analysis is applied. Although some fluid-structure interaction effects were reported (resulting in a HCF life reduction of about 20%), e.g., for the gas turbine blade considered in [7]—with a thickness-to-chord ratio of about 0.2—it is assumed that for the considered reference LRE turbine blade (with a thickness-to-chord ratio of about 0.42), FSI effects are negligible.

2. Numerical Analysis Method

In this section, a complete numerical analysis method for arbitrary full-admission turbine blades is suggested, taking into account HCF and LCF separately. Both of these fatigue-life analysis methods require in the first instance some 3D FE analyses and follow-on (one-way coupled) post-processing analyses for the highest loaded points of the FE mesh.

2.1. LRE Turbine-Blade FE Analysis Method Outline

All of the FE analyses described in the two subsections of this section are based on:

- The usage of a commercial FE program package [8].
- The temperature dependent parameters of the turbine-blade material.
- The geometry of single and two half turbine blades, the related disk section and the related rotor section of the first rotor stage of the considered turbo pump.
- Additionally, all of the structural FE analyses are based on:
  - bi-linear elasto-plasticity with the von Mises yield criterion and kinematic hardening,
  - additive split of the total strain into thermal, elastic, plastic and creep strain,
  - classical three-parameter model approach for taking into account secondary creep (multiplicative combination of Norton's stress power law and the exponential activation energy law) in order to take into account the dependency of the creep strain rate $\dot{\varepsilon}_{creep}$ on both the stress σ and temperature T by means of a single equation, Equation (1), as, e.g., suggested in [9]:

$$\dot{\varepsilon}_{creep} = C_1 \sigma^{C_2} e^{-\frac{C_3}{T}} \tag{1}$$

With:
C_1: multiplicative factor of the Norton stress power law.
C_2: exponent of the Norton stress power law.

$$C_3 = \frac{E_a}{R} \tag{2}$$

With:
E_a: activation energy.
R: gas constant.
The constants C_1, C_2 and C_3 are least-squares fitted by using Equation (8), which is the logarithmic form of Equation (1) to the creep data from [10].

2.1.1. HCF and Creep Related FE Analysis Method

The FE part of the HCF and creep analysis is based on two (one-way coupled) FE analyses:

- A stationary thermal 3D FE analysis, simulating the thermal field during the stationary hot run.
- A quasi-stationary structural 3D FE analysis (with thermal strains calculated from the thermal field of the abovementioned thermal FE analysis) with six load steps $LS_{1,HCF\&creep}$ to $LS_{6,HCF\&creep}$:
  - $LS_{1,HCF\&creep}$ (for the time range $t = 0$ s to $t = 1$ s): thermal strains from the abovementioned stationary thermal FE analysis. Although from the post-processing HCF analysis point of view, this loading could be integrated into load step 3, it is useful to separate it in order to show the negligible influence of the quasi-static thermal loading to the stresses, obtained by the FE model.
  - $LS_{2,HCF\&creep}$ (for the time range $t = 1$ s to $t = 2$ s): additional spin loading (modelling centrifugal forces under high temperature). Although from the post-processing HCF analysis point of view, this loading could be integrated into load step 3, it is useful to separate it in order to show the dominant influence of the spin-loading to the stresses obtained by the FE model.
  - $LS_{3,HCF\&creep}$ (for the time range $t = 2$ s to $t = 3$ s): an additional $0.75 \cdot$ the (circumferential and axial) average gas bending load (originating @ the stator row). This load step results in the minimum stress of the stationary hot run of the turbine and therefore is directly needed for the post-processing HCF analysis of the turbine blade.
  - $LS_{4,HCF\&creep}$ (for the time range $t = 3$ s to $t = 4$ s): an additional $0.5 \cdot$ the (circumferential and axial) average gas bending load (originating @ the stator row). Therefore, load step $LS_{4,HCF\&creep}$ combines full thermal, full centrifugal and $1.25 \cdot$ the (circumferential and axial) average gas bending load (originating @ the stator row). This load step results in the maximum stress of the stationary hot-run of the turbine and therefore is directly needed for the post-processing HCF analysis of the turbine blade.
  - $LS_{5,HCF\&creep}$ (for the time range $t = 4$ s to $t = 540$ s): completely unchanged boundary conditions (for modelling both stress relaxation at the maximum HCF-loaded point and the build-up of radial creep deformation at the tip of the blade for the full duration of the stationary hot run of the turbine). According to [11], the hot-run duration of the reference engine is 540 s.
  - $LS_{6,HCF\&creep}$ (for the time range $t = 540$ s to $t = 542$ s): reduction of thermal strains, spin load, circumferential and axial gas bending loads to zero (for obtaining the residual creep deformation after the end of a single hot run).

For the post-processing HCF analysis discussed in Section 2.2.1, only load steps $LS_{3,HCF\&creep}$ and $LS_{4,HCF\&creep}$ are relevant. The choice of the gas bending forces according to load steps $LS_{3,HCF\&creep}$ and $LS_{4,HCF\&creep}$ is related to a HCF amplitude to mean gas bending load fraction of 0.25 (as suggested in [12] for non-resonant conditions). This requires a careful design of all of the components of the gas generator and the turbo pumps with respect to the natural frequencies of all of these components for the main operating points of the turbo pumps. In case a large number of strongly different turbo pump operating points cannot be avoided, probabilistic methods, e.g., as suggested in [13], will have to be used to assess risks due to turbine-blade resonance conditions.

2.1.2. LCF-Related FE Analysis Method

The FE part of the LCF analysis of the turbine blade is based on two (one-way coupled) FE analyses:

- A fully transient thermal 3D FE analysis of the thermal loading of two complete engine operation cycles with twelve load steps $LS_{1,therm.trans.}$ to $LS_{12,therm.trans.}$. The reason for this two-cycle thermal FE analysis is some shakedown of the cyclic strain, obtained by the follow-on elasto-plastic structural FE analysis from the first to the second loading cycle. The second half $LS_{7,therm.trans.}$ to $LS_{12,therm.trans.}$ of the load steps are identical to the first half $LS_{1,therm.trans.}$ to $LS_{6,therm.trans.}$ of the load steps. Therefore, only the first half $LS_{1,therm.trans.}$ to $LS_{6,therm.trans.}$ of the load steps is described in detail:
  - $LS_{1,therm.trans.}$ (for the time range $t = 0$ s to $t = 1$ s): Linearly ramping up to chill-down boundary conditions ($T_{bulk,impeller} = 36$ K at the impeller position of the FE model while keeping ambient bulk temperature at the surface of the turbine blade).
  - $LS_{2,therm.trans.}$ (for the time range $t = 1$ s to $t = 6300$ s): Keeping identical chill-down boundary conditions as at the end of the previous load step $LS_{1,therm.trans.}$. The chill-down duration (of 105 minutes) is chosen according to [14].
  - $LS_{3,therm.trans.}$ (for the time range $t = 3600$ s to $t = 6301$ s): Linearly ramping up the blade surface bulk temperature to the hot-run condition $T_{bulk,blade} = 800$ K while keeping $T_{bulk,impeller} = 36$ K at the impeller position of the FE model.
  - $LS_{4,therm.trans.}$ (for the time range $t = 6301$ s to $t = 6841$ s): Keeping identical hot-run boundary conditions as in the previous load step $LS_{3,therm,trans.}$. The hot-run duration (of 540 s) is chosen according to [11].
  - $LS_{5,therm.trans.}$ (for the time range $t = 6841$ s *to* $t = 6842$ s): Linearly ramping down the blade surface bulk temperature to ambient condition $T_{bulk,blade} = 295$ K while keeping $T_{bulk,impeller} = 36$ K at the impeller position of the FE model.
  - $LS_{6,therm.trans.}$ (for the time range $t = 6842$ s to $t = 17000$ s) Keeping identical shut-down boundary conditions as in load step $LS_{5,therm.trans.}$. This (relatively long) duration of $LS_{6,therm.trans.}$ was chosen to ensure stationary thermal conditions before the transition to the second full loading cycle.
- For the follow-on (one-way coupled) quasi-stationary structural 3D FE analysis:
  - Thermal strains from the abovementioned thermal FE analysis.
  - Centrifugal forces (during spin up, stationary hot run and spin down).
  - Average gas bending load, originating at the stator row (during spin up, stationary hot run and spin down).

2.2. Post-Processing Fatigue-Life Analysis Methods of LRE Turbine Blades

Both (HCF and LCF) post-processing fatigue-life analysis methods are based on the results of the FE analyses, described in the previous section (with a single full turbine blade, two half turbine blades and the related disk and rotor sections as geometry):

2.2.1. Post-Processing HCF Analysis Method

As first step of the HCF analysis of the turbine blade, the maximum principal stress values $\sigma_{max,princ.,LS_{3,HCF\&creep,}max.space}$ and $\sigma_{max,princ.,LS_{4,HCF\&creep,}max.space}$ of the highest loaded point of the turbine blade are extracted from load steps $LS_{3,HCF\&creep}$ and $LS_{4,HCF\&creep}$ of the HCF-related structural 3D FE analysis (based on the stationary thermal FE analysis of the hot run). Subsequently, the following HCF-relevant stress values of the highest-loaded point of the turbine blade are calculated:

- The mean stress $\sigma_{m,HCF\&creep}$ of the stationary hot run of the turbo pump according to Equation (3):

$$\sigma_{m,HCF\&creep} = \frac{\sigma_{max,princ.,LS_{3,HCF\&creep,.}max.space} + \sigma_{max,princ.,LS_{4,HCF\&creep,}max.space}}{2} \quad (3)$$

- Similarly, the stress amplitude $\sigma_{a,HCF\&creep}$ of the stationary hot run of the turbo pump is calculated according to Equation (4):

$$\sigma_{a,HCF\&creep} = \frac{\sigma_{max,princ.,LS_{4,HCF\&creep},max.space} - \sigma_{max,princ.,LS_{3,HCF\&creep},max.space}}{2} \quad (4)$$

- Finally, the number of HCF cycles to failure $N_{f,HCF}$ is calculated by applying the modified Goodman equation (Equation (5)) as suggested in [15]:

$$N_{f,HCF} = \sqrt[B']{\frac{\sigma_{a,HCF\&creep}}{A'\left(1 - \frac{\sigma_{m,HCF\&creep}}{C'}\right)}} \quad (5)$$

with A', B' and C' as constants, fitted by applying the logarithmized version of Equation (5) to the results of 18 piezo actor driven (ultrasonic) uniaxial HCF tests in total with R > −1 at ambient temperature under high-pressure H_2 atmosphere.

2.2.2. Post-Processing LCF Analysis Method

As some strain-range shakedown from the first to the second full loading cycle of the turbine blade is observed, only the strain values of the second loading cycle are considered.

- As first step of the post-processing LCF analysis of the turbine blade, the minimum over-time and minimum over-all FE mesh node value of the minimum principal total mechanical strain $\varepsilon_{min.princ.,min.2^{nd}cycle,min.space}$ of the turbine blade is extracted from the structural 3D FE analysis of the second full loading cycle (based on the transient thermal FE analysis).
- Subsequently, two of the values this triple minimum is related to are fixed:
  - The (minimum principal strain) direction, which the value $\varepsilon_{min.princ.,min.2^{nd}cycle,min.space}$ refers to;
  - The node of the FE mesh, which the value $\varepsilon_{min.princ.,min.2^{nd}cycle,min.space}$ refers to.
- For these two fixed values (of direction and spatial location), the maximum normal strain $\varepsilon_{fixed-dir.,max.2^{nd}cycle,fixed-loc.}$ of the full second loading cycle is determined.
- Subsequently, the total mechanical strain range $\Delta\varepsilon_{LCF}$ of the highest LCF-loaded point of the turbine blade is calculated according to Equation (6):

$$\Delta\varepsilon_{LCF} = \varepsilon_{fixed-dir.,max.2^{nd}cycle,fixed-loc.} - \varepsilon_{min.princ.,min.2^{nd}cycle,\ min.space} \quad (6)$$

- Finally, the number of LCF cycles to failure $N_{f,LCF}$ of the turbine blade is calculated according to the modified Langer equation (Equation (7)) as suggested in [16]:

$$N_{f,LCF} = 10^{10^{B_0 \log_{10}(\Delta\varepsilon_{LCF} + B_1) + B_2}} \quad (7)$$

with B_0, B_1 and B_2 as constants, determined from a linear regression analysis of the results of (in total) 58 isothermal load controlled or strain controlled fatigue tests with Inconel 718 samples, tested at $T = 811$ K in air environment using induction heating with total strain ranges between 0.5% and 5%, leading to fatigue life values between 100 cycles to 10 Mcycles to failure [16].

3. Material, Material Parameters, Geometry and Loading Conditions

A turbine blade of the 1st rotor row of a gas-generator-driven hydrogen turbo pump [6] of a 1 MN thrust class LRE was selected as reference turbine blade for this paper.

3.1. Material of the Reference Turbine Blade

According to [6]:

- "Super Waspaloy" was foreseen as blade material in the initial phase of the development;
- However, for cost efficiency reasons, Inconel 718 was selected at a later stage of the development of the turbo pump of the 1 MN thrust class gas-generator reference LRE.

3.2. Material Parameters of the Reference Turbine Blade

In this section, both thermal and structural parameters of the reference turbine-blade material (Inconel 718) are given.

3.2.1. Thermal FE Analysis Parameters of the Reference Turbine-blade Material

As shown in Figures 1 and 2, temperature-dependent parameters for modelling thermal expansion and heat capacity of the turbine-blade material were used for the FE analyses, shown in Section 4 of this paper.

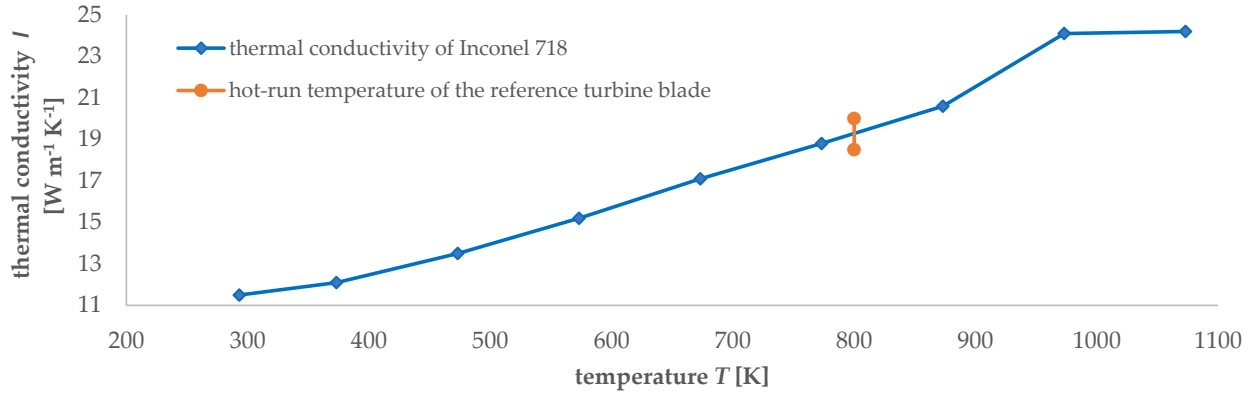

Figure 1. Temperature−dependent thermal conductivity of the blade material of the reference turbo pump as taken from [17].

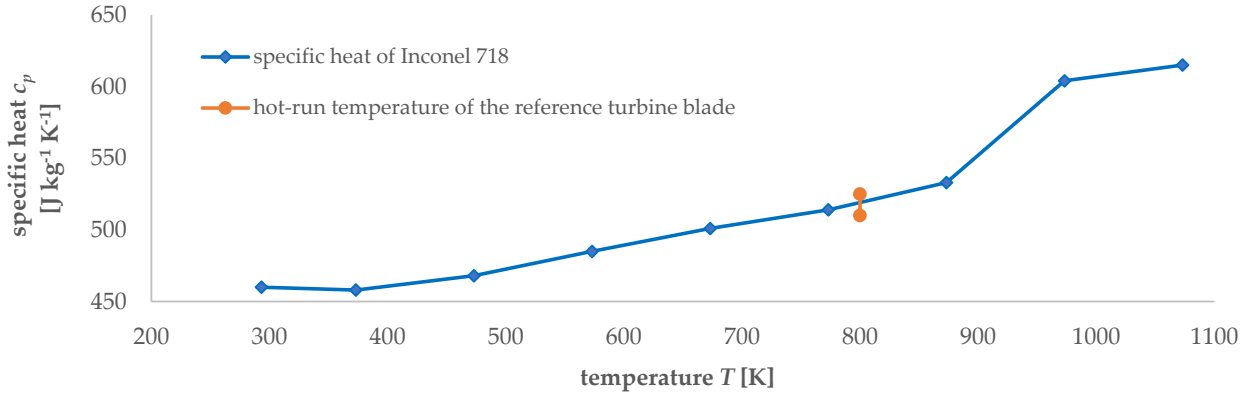

Figure 2. Temperature−dependent specific heat of the blade material of the reference turbo pump according to [17].

3.2.2. Structural FE Analysis Parameters of the Reference Turbine-blade Material

As shown in Figures 3–6, temperature-dependent material parameters, both for modelling elasto-plasticity and for modelling creep, were used for the structural FE analyses, as shown in Section 4.

The values of the creep parameters C_1 to C_3 according to Equation (1) are given in Table 1.

Table 1. Parameters used for modelling creep according to Equation (1).

Creep Parameter	Value	Unit
C_1	$4.539 \cdot 10^{-105}$	$s^{-1}MPa^{-C_2}$
C_2	15.57	-
C_3	$8.677 \cdot 10^4$	K

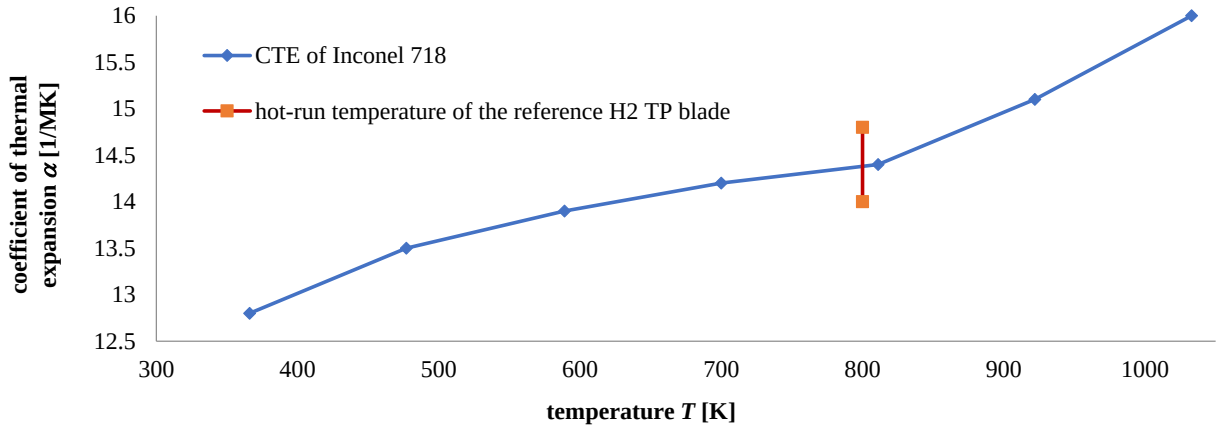

Figure 3. Temperature−dependent coefficient of thermal expansion (CTE) of the blade material of the reference turbo pump according to [18].

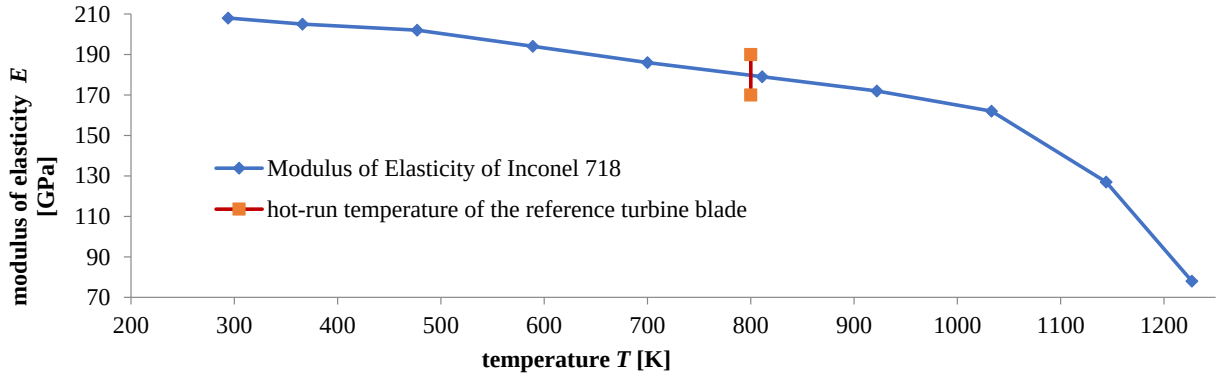

Figure 4. Temperature−dependent modulus of elasticity of the blade material of the reference turbo pump according to [18].

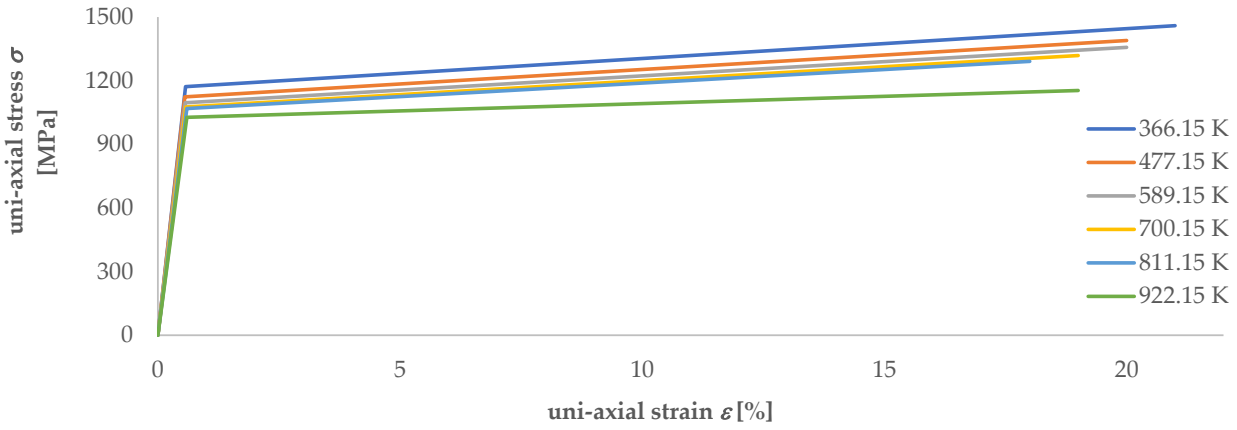

Figure 5. Assumed temperature−dependent bi-linear elasto−plastic behavior of the blade material (Inconel 718) of the reference turbo pump according to [18].

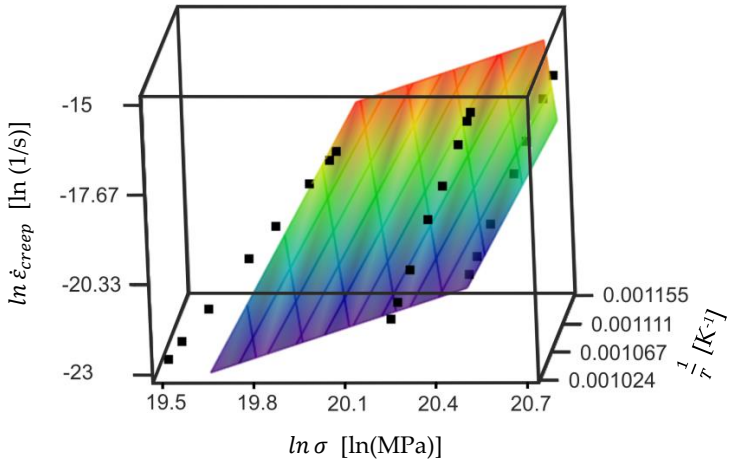

Figure 6. Colored plane: $ln-$transformed secondary creep behavior of the blade material (Inconel 718) of the reference turbo pump; black squares: data from [10], used for least squares fitting the 3 parameters of Equation (1) by using the bilinear Equation (8).

As shown in Equation (8), the (originally non-linear) creep Equation (1) becomes bi-linear, when:

- The natural logarithm is applied to Equation (1), resulting in Equation (8):

$$ln\dot{\varepsilon}_{creep} = lnC_1 + C_2 ln\sigma - \frac{C_3}{T} \tag{8}$$

- And $ln\sigma$ and $\frac{1}{T}$ are used as dependency (input) parameters for obtaining the natural logarithm of the creep strain rate $ln\dot{\varepsilon}_{creep}$ as a function value of Equation (8).

The bi-linearity of the ln-transformed creep model according Equation (8) is visualized in Figure 6.

The structural analysis parameters, which are not temperature dependent, are summarized in Table 2:

Table 2. Temperature−independent structural analysis parameters.

Structural Analysis Parameter	Value	Unit
Poisson's ratio ν	0.31	-
Density ϱ	8192	kg/m^3

3.2.3. Fatigue-Life Analysis Parameters of the Reference Turbine-Blade Material

In this section, the Inconel 718 parameters for both the HCF analysis and the LCF analysis of the reference turbine blade are given.

HCF Analysis Parameters of the Reference Turbine-Blade Material

The (high-pressure GH_2-test-related) HCF analysis parameters for Inconel 718, needed for applying Equation (5), are:

- Summarized in Table 3;
- Available (from [15]) for ambient temperature only.

LCF Analysis Parameters of the Reference Turbine-Blade Material

The LCF analysis parameters for Inconel 718, needed for applying Equation (7), are:

- Available (from [16]) for a series of temperatures;
- Summarized in Table 4 for $T = 811$ K.

Table 3. Ambient temperature, high-pressure GH_2-test-related parameters of Inconel 718, applied to the HCF analysis according to Equation (5).

HCF Analysis Parameter	Value	Unit
A'	15,168	MPa
B'	−0.2451	-
C'	1089	Mpa

Table 4. Inconel 718 parameters for $T = 811$ K, as used for the LCF analysis of the turbine blade according to the modified Langer equation (Equation (7)).

LCF Analysis Parameter	Value	Unit
B_0	−0.3553	-
B_1	−0.4582	-
B_2	0.5357	-

3.3. Assumed Turbine-Blade Geometry

Due to the very low density of LH_2, both a larger rotational speed and larger turbine power (in comparison to the LOX turbopump) are necessary for the LH_2 turbopump of LOX + LH_2 LREs (although the hydrogen mass-flow rate is just a relatively small fraction of the total propellant mass-flow rate). Therefore, the blade of a LH_2 turbopump is selected as a (worst-case) reference turbine blade. Furthermore, a turbine blade of the 1st rotor stage of a two-stage turbopump can be assumed (for the following reasons) as the higher loaded turbine blade (in comparison to the blade of the 2nd rotor stage):

- Highest temperature directly from the gas generator or (in case of other engine cycles) the pre-burner or the (expander LRE) cooling circuit (and therefore, usually most severely thermally reduced material properties);
- Highest share of the total turbine work [19].

Therefore, a turbine blade from the 1st rotor row of a two-stage LH_2 turbine was selected as reference turbine blade for this paper.

Although quite a few publications are available describing the turbopumps of 1 MN thrust class gas generator LREs [6,19,20], these do not contain the complete geometric data of the turbine blades. Therefore, most of the geometric data of the reference turbine blade (such as leading- and trailing-edge radii and the cross-section geometry of the turbine blade) were taken from [21]. The geometric values, extracted from [6,21], are summarized in Table 5.

Table 5. Geometric data of the (1 MN thrust class gas generator LRE related) reference turbine blade.

Geometric Parameters	Value	Unit	Reference
Mean blade diameter d_{mean}	240	mm	[6]
Number $n_{1st\ stator\ row}$ of blades of the 1st stator row	23	-	[6]
Number $n_{1st\ rotor\ row}$ of blades of the 1st rotor row	106	-	[6]
Total height h of the blade	12.5	mm	[21]
Leading edge radius r_{lead} of the blade (r1 as shown in Figure 7)	0.209	mm	[21]
Trailing edge radius r_{trail} of the blade (r2 as shown in Figure 7)	0.157	mm	[21]
Transition radius r_{fillet} disk—blade (fillet radius)	0.55	mm	[21]
Blade thickness t (full circle shown in Figure 7)	3.8	mm	[21]
Chord length c of the blade	9	mm	[21]

The cross section of the turbine blade of the 1st rotor stage of the 1 MN thrust class gas generator LRE reference hydrogen turbo pump is shown in Figure 7. This cross section was pieced together from the leading- and trailing-edge radii, the blade thickness and the

chord length given in Table 5 and from a cross-section drawing, extracted from [21]. The cross section shown in Figure 7 (composed of six circle sections and two straight lines) is C^1-continuous (that means, a closed turbine-blade cross-section curve is ensured and sharp corners are avoided in the cross-section curve, but discontinuities of the curvature radii of the abovementioned 6 circle sections and two straight lines are accepted).

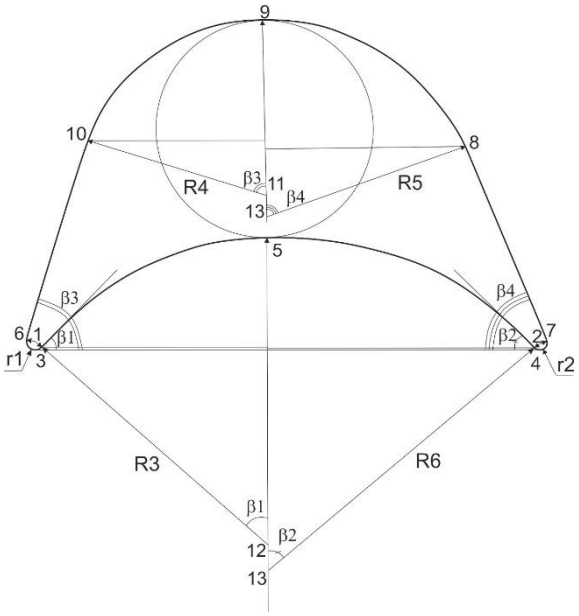

Figure 7. C^1-continuous cross section of the selected turbine blade (with blade thickness indicated by full inner circle, leading edge radius r1 and trailing edge radius r2).

3.4. Assumed Turbine-Blade Loading Conditions

The loading conditions of the reference turbine blade (as extracted from [6,19,21,22]) are summarized in Table 2.

The average blade driving load of each of the blades (caused by supersonic jets emitted by the stator row) in circumferential direction was determined from the number of turbine blades and the total power of the 1st stage of turbine (both given in Table 6) and from the mean blade speed.

Table 6. The 1st rotor row blade loading conditions of the hydrogen turbo pump of the 1 MN thrust class gas generator reference LRE.

Loading Conditions	Value	Unit	Reference
Total temperature at the inlet of the 1st turbine stage (related to the global/fixed coordinate system)	873	K	[6]
Rotational speed n of the reference LRE H_2 turbo pump	35.68	krpm	[6]
Rotational speed ω_{rad} of the reference LRE H_2 turbo pump (as calculated from the line above)	3736	rad/s	-
Output power $P_{out,total}$ of the reference LRE hydrogen turbine	14.29	MW	[6]
Relative power split between the 1st and the 2nd rotor stage of the 1 MN thrust class gas generator LRE hydrogen turbo pump.	60:40	%	[19]
Output power $P_{out,1st\ stage}$ of the 1st stage of the 1 MN thrust class reference LRE hydrogen turbine (as calculated from the two table lines above)	8574	kW	-
Quotient: Total temperature, related to the relative (rotating) coordinate system of the turbine blade/total temperature, related to the global (fixed) coordinate system	0.917	-	[21]
Total temperature in the relative (rotating) coordinate system of the turbine blade of the 1st rotor stage (as calculated from the very 1st and the above-line of this table)	800	K	-
Static pressure at the inlet of the 1st rotor stage of the 1 MN thrust class reference H_2 turbo pump	4.18	MPa	[21]

Table 6. *Cont.*

Loading Conditions	Value	Unit	Reference
Static pressure at the outlet of the 1st rotor stage of the 1 MN thrust class reference H_2 turbo pump	3.57	MPa	[21]
Mean static pressure of the 1st rotor stage of the 1 MN thrust class reference H_2 turbo pump (as calculated from the two table lines above)	3.88	MPa	-
Total temperature at the H_2 inlet of the 1 MN reference thrust chamber (assumed as total temperature at the H_2 outlet of the 1 MN reference H_2 turbo pump, and therefore applied as impeller temperature of the turbo pump)	36	K	[22]

3.5. Boundary Conditions of the Reference Turbine Blade

The authors of this paper are aware that a 3D CFD analysis of the flow of the turbine driving gas, fully (two-way) coupled with a 3D thermal FE analysis of the heat conduction in the blade and related disk and rotor sections, would provide the most accurate thermal boundary conditions for the follow-on (structural FE and post-processing fatigue life) analyses. However, the main focus of the work shown in this paper was put on the thermal FE, structural FE and post-processing fatigue-life analysis of the reference turbine blade. Instead of running a CFD analysis for a high-end modelling of the heat transfer, simplified thermal boundary conditions were applied.

3.5.1. Boundary Conditions for the HCF- and Creep-Related FE Analyses

In this subsection, the boundary conditions of the reference turbine blade and related disk and rotor sections are given of both the stationary thermal FE analysis of the hot-run and the quasi-stationary structural FE analysis of the full loading cycle.

Boundary Conditions for the Stationary Thermal FE Analysis of the Reference Turbine Blade

Although the full disk and all of the turbine blades are in contact with the (hot) turbine driving gas, the turbine driving gas velocity (and as result, the film coefficient) is assumed to have a large value in the vicinity of the blades only. Therefore, adiabatic boundary conditions are assumed on all of the disk and rotor sections with the following two exceptions:

The yellow faces, shown on the lefthand side of Figure 8, indicate convective boundary conditions with the following bulk temperatures:

- A: The impeller temperature (36 K);
- B: The total temperature of the turbine driving gas (from the gas generator) in the local coordinate system of the blade (800 K).

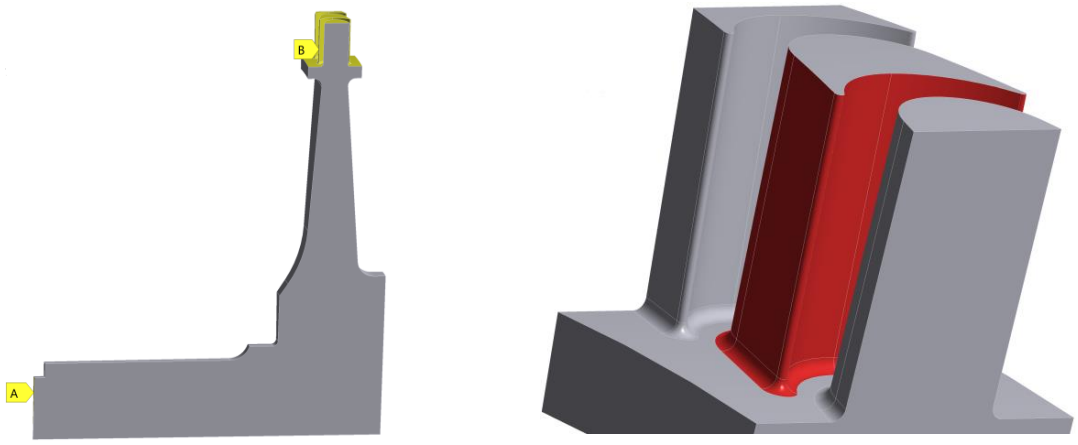

applied thermal boundary conditions static and gas bending pressure boundary conditions

Figure 8. (**Left**): convective boundary condition faces of the thermal FE analyses; (**right**): turbine-blade driving-gas-related pressure boundary of the structural FE analysis.

The complete convective boundary conditions related to the yellow faces A and B, shown on the lefthand side of Figure 8, are given in Table 7.

Table 7. Boundary conditions for the stationary thermal FE analysis of the hot-run of the reference turbine blade.

	Impeller Position Boundary [Face A of Figure 8]	**Blade and Outer Disk Surface Boundary [Face B of Figure 8]**
bulk temperature T_{bulk} [K]	36	800
film coefficient h_{film} [kWm^{-2} K^{-1}]	1000	50

Boundary Conditions for the HCF- and Creep-Related Quasi-Stationary Structural FE Analysis of the Reference Turbine Blade

The boundary conditions for the quasi-stationary structural FE analysis of the turbine blade are given in Table 8.

Table 8. Structural boundary conditions for the quasi-stationary structural FE analysis of a single HCF loading cycle and full hot-run duration creep of the reference turbine blade.

Load Step Number	**Time Range of the Load Step [s]**	**Spin Loading [rad/s]**	**Static Pressure (Normal to the Surface) [MPa]**	**Component Pressure, Acting in Axial Direction of the Turbine [MPa]**	**Component Pressure, Acting in Circumferential Direction of the Turbine [MPa]**
$LS_{1,HCF\&creep}$	0–1	0	0	0	0
$LS_{2,HCF\&creep}$	1–2	3736	0	0	0
$LS_{3,HCF\&creep}$	2–3	3736	3.88	0.112	0.377
$LS_{4,HCF\&creep}$	3–4	3736	3.88	0.186	0.629
$LS_{5,HCF\&creep}$	4–540	3736	3.88	0.186	0.629
$LS_{6,HCF\&creep}$	540–542	0	0	0	0

All of the pressure values given in Table 8 are applied to the red face shown on the righthand side of Figure 8. The static pressure (as given in the center column of Table 8) is set to the mean static pressure of the reference turbine blade as given in Table 6. The component pressure in axial direction of the turbine (as given in the center-right column of Table 8) was adjusted to the turbine driving-gas pressure drop of the reference turbine-blade rotor stage. The component pressure in circumferential direction of the turbine (as given in the righthand side column of Table 8) was adjusted to the power a single reference turbine blade contributes to the total power of the reference turbo pump.

3.5.2. Boundary Conditions for the LCF-Related FE Analyses

In this subsection, the boundary conditions of the reference turbine blade and related disk and rotor sections of a single full loading cycle are given for both the transient thermal FE analysis and for the follow-on quasi-static structural FE analysis.

Boundary Conditions for the Transient Thermal FE Analysis of the Reference Turbine Blade

The boundary conditions for the transient thermal FE analysis of the reference turbine blade are summarized in Table 9.

Boundary Conditions for the LCF-Related Quasi-Stationary Structural FE Analysis of the Reference Turbine Blade

The boundary conditions for the LCF-related quasi-stationary structural FE analysis of the turbine blade are given in Table 10.

Table 9. Boundary conditions for the transient thermal FE analysis of a single loading cycle of the reference turbine blade.

		Impeller Position Boundary [Face A of Figure 8]		Blade and Outer Disk Surface Boundary [Face B of Figure 8]	
Load Step Number	**Time Range t of the Load Step [s]**	**Bulk Temperature $T_{bulk,impeller}$ [K]**	**Film Coefficient $h_{film,impeller}$ [kWm^{-2} K^{-1}]**	**Bulk Temperature $T_{bulk,blade}$ [K]**	**Film Coefficient $h_{film,blade}$ [kWm^{-2} K^{-1}]**
$LS_{1,therm.trans.}$	0–1	36	1000	295	0.2
$LS_{2,therm.trans.}$	1–6300	36	1000	295	0.2
$LS_{3,therm.trans.}$	6300–6301	36	1000	800	50
$LS_{4,therm.trans.}$	6301–6841	36	1000	800	50
$LS_{5,therm.trans.}$	6841–6842	36	1000	295	0.2
$LS_{6,therm.trans.}$	6842–17,000	36	1000	295	0.2

Table 10. Structural boundary conditions for the LCF-related quasi-stationary structural FE analysis of a full hot run of the reference turbine blade.

Load Step Number	**Time Range of the Load Step [s]**	**Spin Loading [rad/s]**	**Static Pressure (Normal to the Surface) [MPa]**	**Component Pressure, Acting in Axial Direction of the Turbine [MPa]**	**Component Pressure, Acting in Circumferential Direction of the Turbine [MPa]**
$LS_{1,LCF}$	0–1	0	0	0	0
$LS_{2,LCF}$	1–6300	0	0	0	0
$LS_{3,LCF}$	6300–6301	3736	3.88	0.112	0.377
$LS_{4,LCF}$	6301–6841	3736	3.88	0.186	0.629
$LS_{5,LCF}$	6841–6842	0	0	0	0
$LS_{6,LCF}$	6842–17,000	0	0	0	0

The load steps $LS_{7,LCF}$ to $LS_{12,LCF}$, modelling the 2nd full loading cycle of the turbine (in the time range $t = 17000$ s to $t = 34000$ s) are identical to load steps $LS_{1,LCF}$ to $LS_{6,LCF}$.

3.6. FE Meshing of the Reference Turbine Blade

The meshing of all of the (thermal, structural, transient and stationary) FE analyses described in this paper is shown in Figure 9. The mesh zoom in the center of Figure 9 shows the highest HCF-loaded area of the reference turbine blade (transition from the leading edge of the turbine blade to the disk. The mesh zoom on the righthand side of Figure 9 shows the highest LCF-loaded area of the reference turbine blade (transition from the suction side of the turbine blade to the disk.

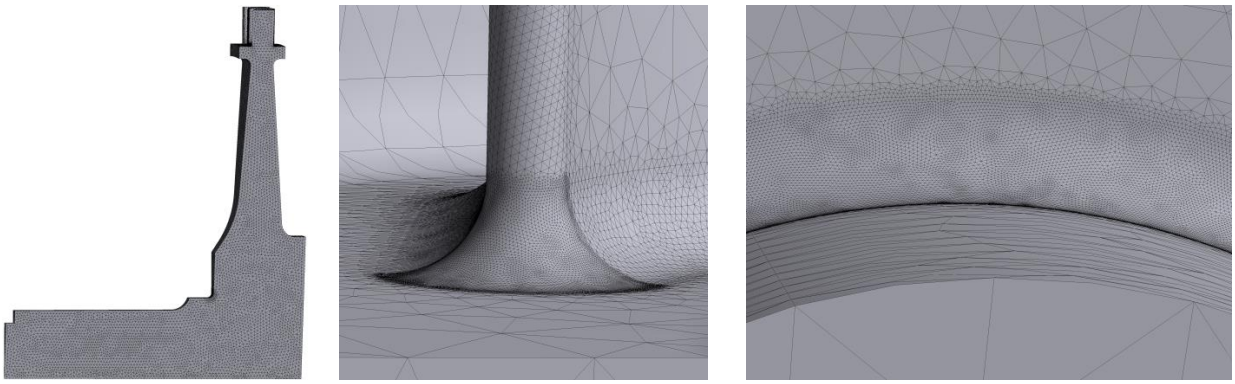

full FE mesh FE mesh @ highest-HCF-loaded area FE mesh @ highest LCF-loaded area

Figure 9. Mesh, used for all of the finite element analyses of the reference turbine blade and the related disc and rotor section; lefthand side: full FE mesh; center and righthand side: FE mesh zooms in the vicinity of the highest HCF- and LCF-loaded areas, respectively.

4. Results

In this section, both FE-analysis results and post-processing fatigue-life analysis results are shown for the selected reference turbine blade.

4.1. FE Analysis Results

In this section, the results of both the thermal FE analysis and structural FE analysis of the reference turbine blade are shown.

4.1.1. Thermal FE Analysis Results

In this section the results of both the stationary and the transient thermal FE analysis of the reference turbine blade are shown.

Results of the (HCF-Related) Stationary Thermal FE Analysis of the Reference Turbine Blade

The main result of the stationary thermal FE analysis of the reference turbine blade and the related disk and rotor section is shown in Figure 10.

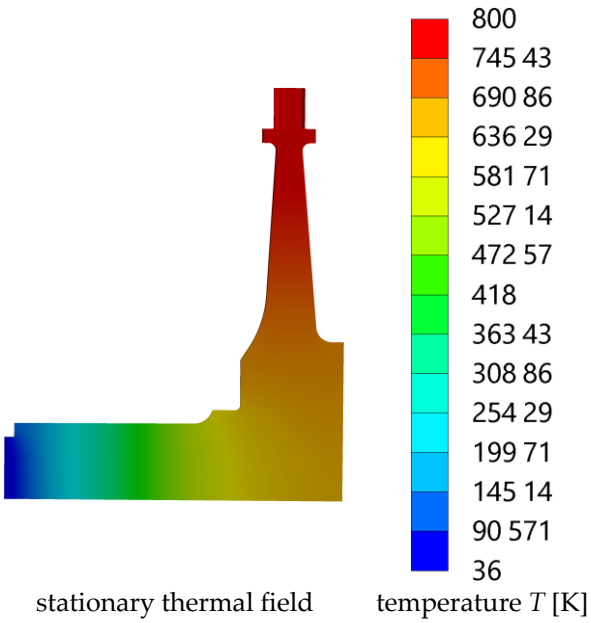

Figure 10. Main result of the stationary thermal FE analysis of the hot run of the reference turbine blade and the related disc and rotor section.

The stationary thermal field of the turbine blade (as shown in Figure 10) is the main input for the two follow-on analyses:

- directly for the structural FE analysis of the (from the thermal point of view, stationary) hot run of the turbo pump (as shown in Section 4.1.2),
- indirectly also for the post-processing HCF analysis of the reference turbine blade (as shown in Section 4.2).

Based on the thermal field shown in Figure 10, the thermal strains are calculated (by multiplying the difference between the thermal field and the reference temperature by the coefficient of thermal expansion.

Results of the (LCF-Related) Transient Thermal FE Analysis of the Reference Turbine Blade

The main results of the (LCF-related) transient thermal FE analysis of the reference turbine blade and the related disk and rotor section are shown in Figures 11 and 12.

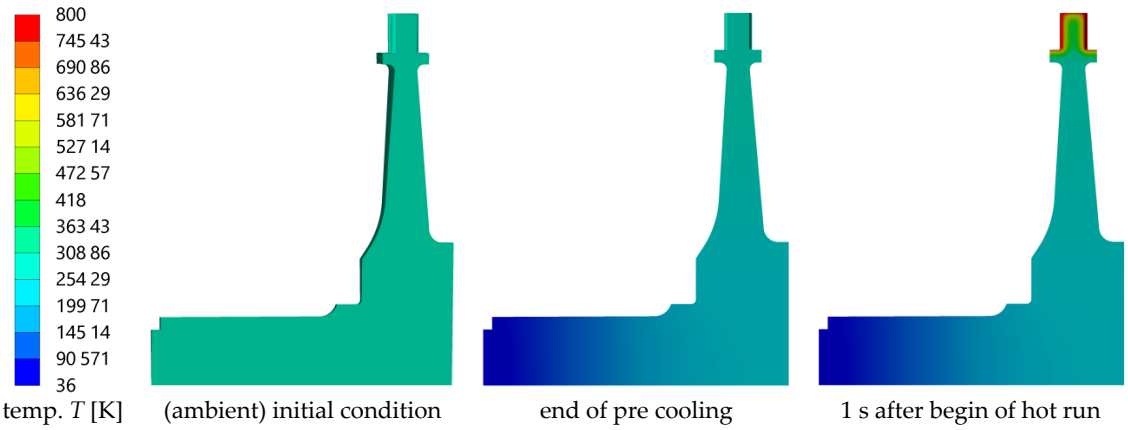

Figure 11. Thermal fields of the reference turbine blade and related disk and rotor section at selected points in time (at pre cooling and start-up of the turbo pump).

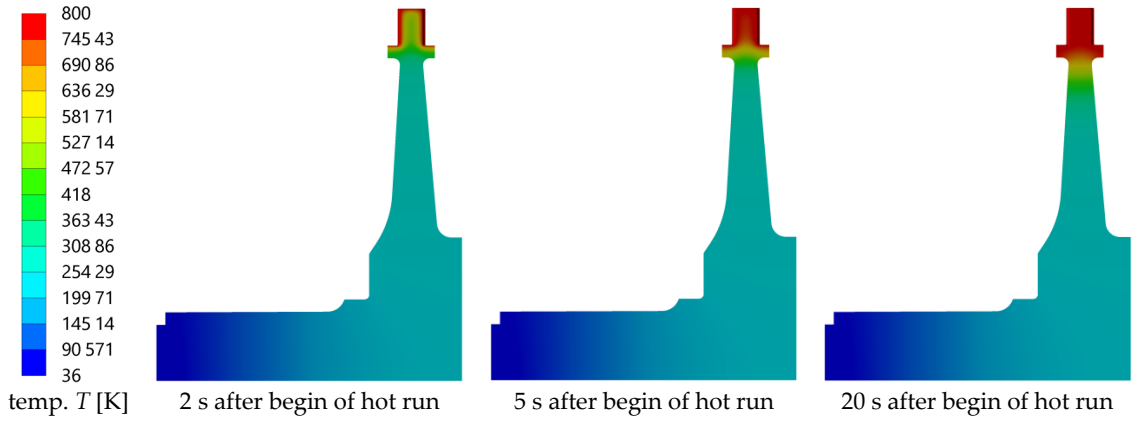

Figure 12. Thermal fields of the reference turbine blade and related disk and rotor section at selected points in time (early phase of the hot run of the engine).

In Figure 13, the variation in time of the temperature of the maximum-LCF-loaded point is shown.

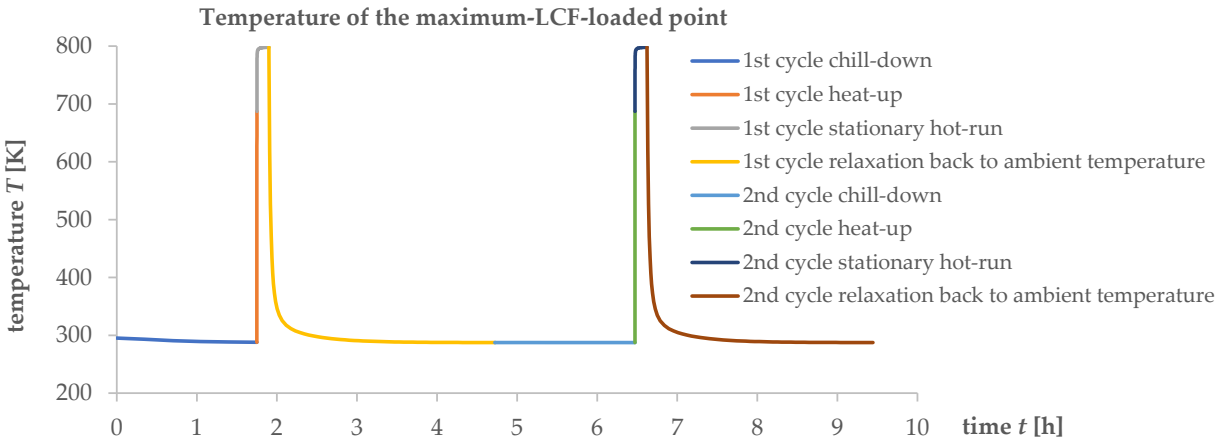

Figure 13. Variation in time of the temperature of the highest LCF-loaded point (transition from the suction side of the blade to the disk).

The transient thermal field of the turbine blade (as shown in Figures 11–13) is the main input for the two follow-on analyses:

- directly for the quasi-stationary structural FE analysis of the complete operating cycle of the turbo pump (pre-cooling, start-up, stationary hot-run, and shut-down of the turbo pump as shown in Section 4.1.2); from the time-dependent thermal field shown in Figures 11 and 12, the thermal strains of the structural analysis are calculated (by multiplying the difference between the thermal field and the reference temperature by the coefficient of thermal expansion),
- indirectly for the post-processing LCF analysis of the reference turbine blade (as shown in Section 4.2).

4.1.2. Results of the Quasi-Stationary Structural FE Analysis of the Reference Turbine Blade

In this section, the results of two different quasi-stationary structural FE analyses of the reference turbine blade are shown: the first one based on the stationary thermal field (as shown in Results of the (HCF-Related) Stationary Thermal FE Analysis of the Reference Turbine Blade), the second one based on the transient thermal field of the reference turbine blade (as shown in Results of the (LCF-Related) Transient Thermal FE Analysis of the Reference Turbine Blade).

Results of the HCF-Related Structural FE Analysis

The distributions of the maximum principal stress of the reference turbine blade for the two HCF-relevant load cases $LS_{3,HCF\&creep}$ and $LS_{4,HCF\&creep}$ are shown in Figure 14.

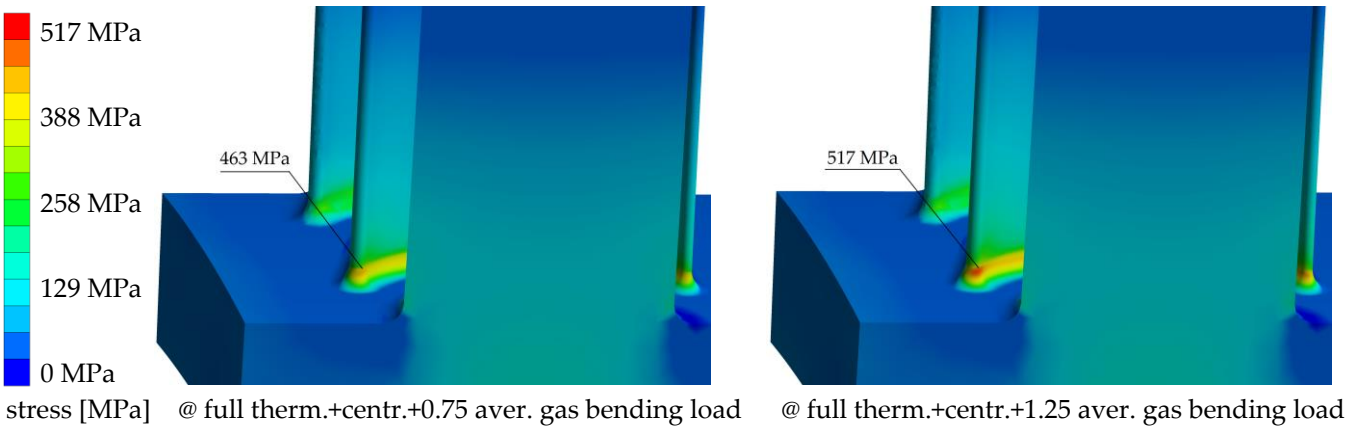

Figure 14. Distribution of the maximum principal stress of the reference turbine blade for the two HCF-determining load cases $LS_{3,HCF\&creep}$ and $LS_{4,HCF\&creep}$—including position locator of the maximum HCF loading point (located at the transition between the leading edge of the blade and the disk).

The HCF-related FE analysis results of the maximum loading point of the 3D model (transition between the leading edge of the blade and the disk) are summarized in Table 11.

Table 11. Maximum loading point results, obtained by the HCF-related 3D FE analysis.

Result Description	3D FE Analysis Value	Unit
Maximum principal stress $\sigma_{max,princ.,LS_{3,HCF\&creep}}$ as obtained by load step $LS_{3,HCF\&creep}$ of the FE analysis at the maximum loading point of the 3D model.	463	MPa
Maximum principal stress $\sigma_{max,princ.,LS_{4,HCF\&creep}}$ as obtained by load step $LS_{4,HCF\&creep}$ of the FE analysis at the maximum loading point of the 3D model.	517	MPa
Cyclic stress $\sigma_{c,HCF\&creep}$ of the stationary hot-run at the maximum loading point.	54	MPa
Stress amplitude $\sigma_{a,HCF\&creep}$ of the stationary hot-run at the maximum loading point.	27	MPa
Mean stress $\sigma_{m,HCF\&creep}$ of the stationary hot-run at the maximum loading point.	490	MPa

In addition to the fatigue-life-related FE analysis results, such as the maximum principal stress at the maximum loading point of the turbine blade as shown in Figure 14, the deflection of the turbine blade is also of interest (e.g., for cross-checking whether the deflection of the turbine blade would be large enough to necessitate a fully coupled thermal–structural interaction FE analysis. The deflection in circumferential direction of the tip of the reference turbine blade is shown in Figure 15.

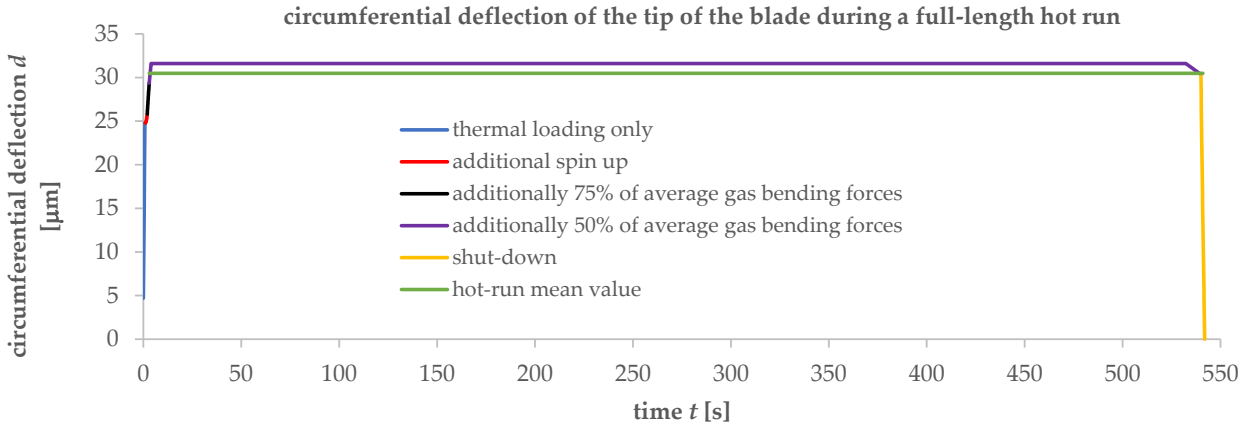

Figure 15. Variation in time of the circumferential deflection of the tip of the reference turbine blade as result of the HCF- and creep-related FE analysis.

Additionally to the variation in time of the circumferential deflection of the tip of the reference turbine blade, the diagram also contains (as horizontal green line) the mean circumferential deflection of the turbine blade during the stationary hot run. As the maximum circumferential deflection of the tip of the reference blade (purple line in Figure 15) is just 1.12 µm larger than the abovementioned mean circumferential deflection, possible fluid–structure interaction effects can be ruled out. This confirms the validity of the applied one-way coupling of the structural FE analysis to the thermal FE analysis.

Creep-Related Results of the Structural FE Analysis

The equivalent creep strain and the maximum principal stress of the maximum-HCF-loaded point (at the transition from the leading edge to the disk as shown in red on the righthand side of Figure 14) are plotted in Figure 16.

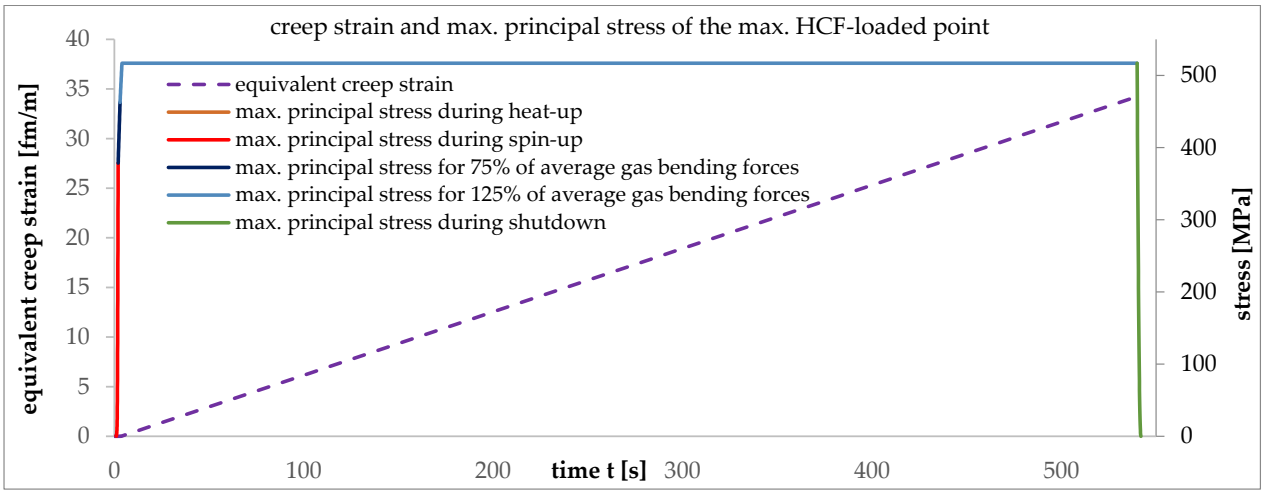

Figure 16. Equivalent creep strain and maximum principal stress of the highest HCF−loaded point for a single full operating cycle of the reference turbo pump.

As indicated by the dashed purple line in Figure 16, the creep strain of the maximum HCF-loaded point grows linearly during the stationary hot run of the turbine. This constant creep strain rate is consistent with the almost constant maximum principal stress at the same point as indicated by the blue solid line of Figure 16. The small total value of the equivalent creep strain $\varepsilon_{creep,equiv.,LS5,HCF\&creep} = 3.42 \cdot 10^{-12}\%$ at the end of the hot-run load step indicates that (due to the moderate thermal loading condition of the reference turbine blade), creep is negligible for the reference turbine blade. This is confirmed by the tiny value of the maximum radial deformation $d_{radial,max,LS6,HCF\&creep} = 1.26$ nm of the tip of the turbine blade after all of the thermal and mechanical loads have been removed at the end of load step $LS_{6,HCF\&creep}$. A large value of $d_{radial,max,LS6,HCF\&creep}$ would indicate the risk of contact/scratching of the turbine blade at the outer housing of the turbine.

Results of the LCF-Related Structural FE Analysis

The main driver for the elasto-plastic LCF-related deformation of the turbine-blade material during the start-up of the turbine is a combined heat capacity and thermal delay effect; due to the large velocity—and therefore also large film coefficient—of the hot turbine driving gas at the surface of the blade, the blade is heated up rapidly by the hot turbine driving gas in the vicinity of the blade surface. However, due to both the non-zero heat capacity and the moderate thermal conductivity of the blade material, the center of the blade remains at its pre cooling temperature at about 1 s after the start-up of the turbine as shown on the righthand side of Figure 11. As a result, the (still small) global thermal deformation of the blade is dominated by its cool center—causing a compressive elasto-plastic deformation of the blade material in the vicinity of the blade surface to compensate for the large tensile thermal strains at these positions. For this reason, the main LCF driver is the minimum principal strain. The minimum principal strain reaches its minimum value at about 9 s after the start of the second hot run of the turbine. For this point in time, the distribution of the minimum principal strain obtained by the LCF-related quasi-stationary structural finite element analysis is shown in Figure 17.

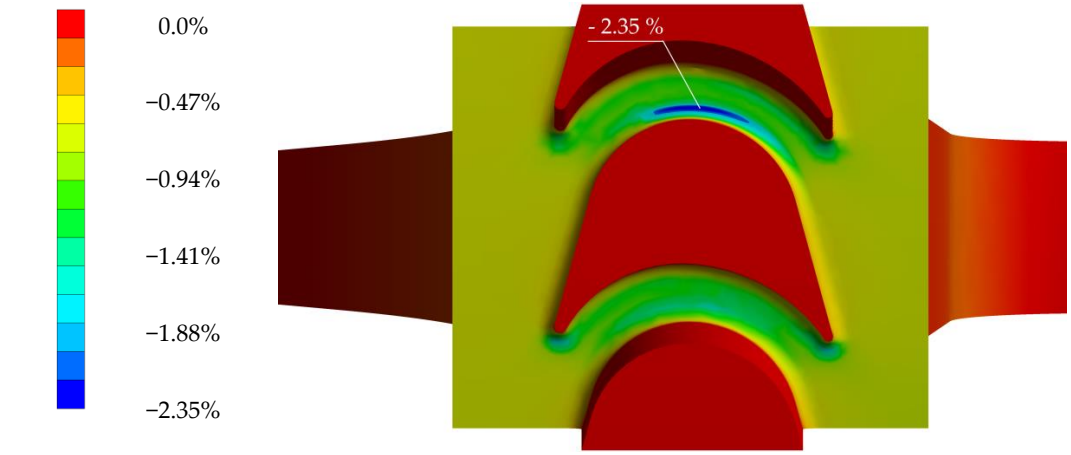

Figure 17. Distribution of the minimum principal strain about 9 s after the 2nd start−up of the turbine.

The stress–strain diagram of the highest LCF-loaded point (transition between the disk and the suction side of the reference turbine blade as indicated by the white annotation line in Figure 17) for hot runs one and two is shown in Figure 18.

The variation in time of the strain of the highest LCF-loaded point shown in Figure 19 (with the same blade-loading-phase color scheme as in Figure 18) eases the separation of the stress–strain values of the first and the second loading cycle plotted in Figure 18.

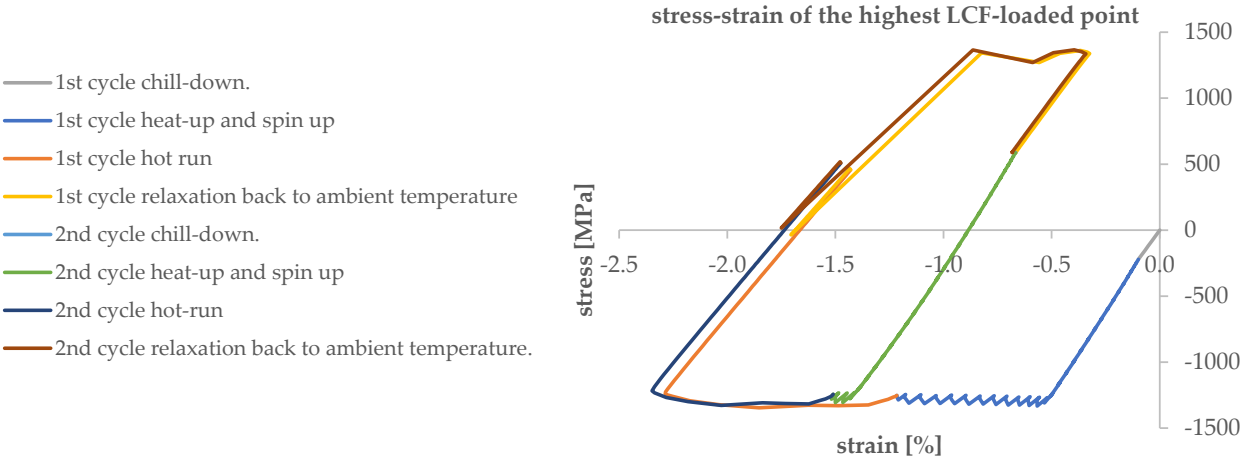

Figure 18. Stress–strain diagram of the highest LCF−loaded point for hot runs 1 and 2.

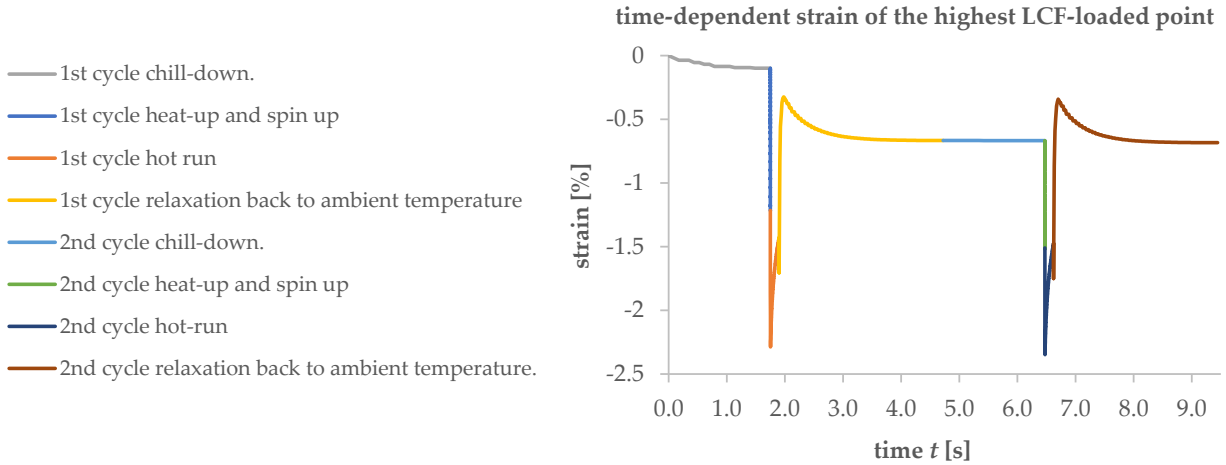

Figure 19. Variation in time of the strain of the highest LCF−loaded point for hot runs 1 and 2.

As shown in [23], no shakedown is obtained by the structural finite element analysis from cycle number two onwards, and therefore, the strain result of the complete second loading cycle can be assumed to be sufficient for the follow-on (post-processing) LCF analysis of the turbine blade.

4.2. Post-Processing Fatigue Life Analysis Results

In this section, the post-processing fatigue-life analysis results of the reference turbine blade for both HCF and LCF are shown.

4.2.1. Post-Processing HCF Analysis Results of the Reference Turbine Blade

Applying the modified Goodman Equation (5) and the (high-pressure-hydrogen-related) values of A', B' and C' given in Table 3 to the FE-analysis results, summarized in Table 11, gives a HCF life of about 14.2 Gcycles to failure. A multiplication of the number of blades in the first stator row (of 23) with a rotational speed of 35.68 krpm results in about 821 thousand load changes per hot-run minute. For the hot-run duration of the reference turbo pump (of—according to [11]—9 min), this results in about 7.38 million HCF cycles per hot run. Putting these abovementioned numbers together results in about 1919 full-length hot runs to HCF failure.

In Figure 10, both the mean stress and the stress amplitude of the 1 MN thrust class gas-generator LRE reference turbine blade are visualized (as the green and purple lines, respectively) in the Haigh diagram of Inconel 718 (taken from [15]).

The HCF iso lines in Figure 20 were calculated (for 100 Mcycles, 1 Gcycle and 10 Gcycles to failure) by applying Equation (5) to the (high-pressure-hydrogen-related) values of A', B' and C' given in Table 3.

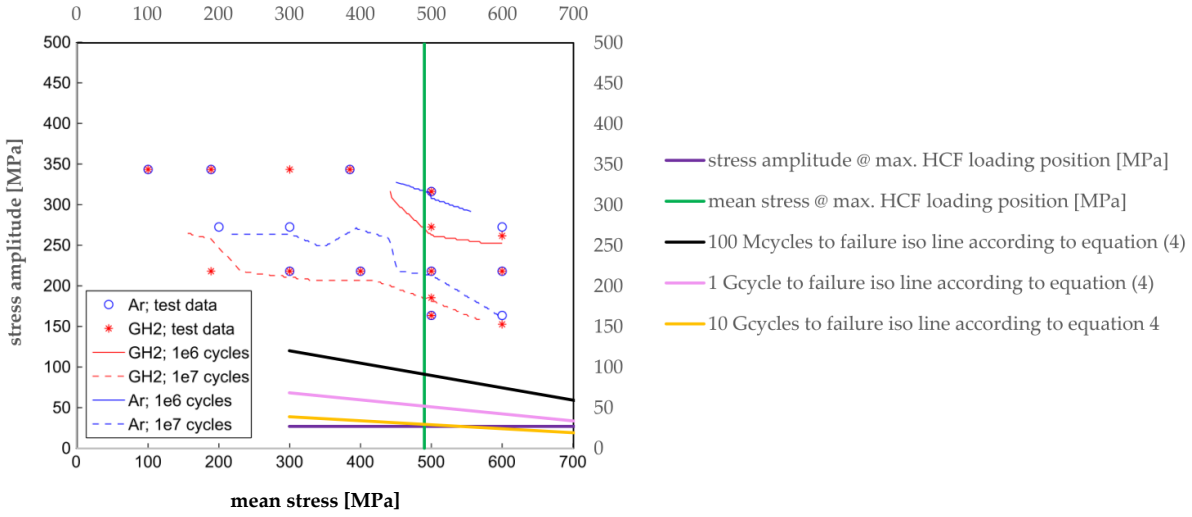

Figure 20. Two-diagram overlay: (a) green and purple lines: HCF conditions of the 1 MN thrust class gas generator LRE reference turbine blade as summarized in Table 11; (b) blue and red lines: Haigh diagrams from [15] for inert gas and hydrogen environmental test conditions, respectively.

4.2.2. Post-Processing LCF Analysis Results of the Reference Turbine Blade

By calculating (for loading cycle number two) the difference between the maximum and the minimum strain value from the diagram, visualized in Figure 18, a cyclic strain value of 2.0% is obtained for the highest LCF-loaded point of the reference turbine blade (located in the transition area between the disk and the suction side of the reference turbine blade).

Using this value as input for the modified Langer Equation (7) results in a post-processing-determined LCF life of about 870 hot runs to failure. The related Langer diagram of Inconel 718 is shown in Figure 21.

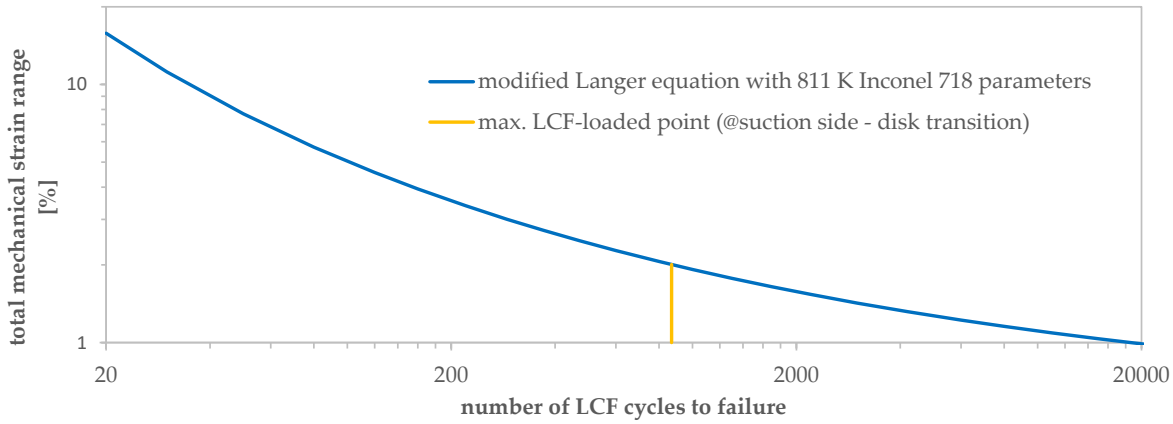

Figure 21. Modified-Langer-equation-based LCF analysis of the highest LCF−loaded point of the reference turbine blade (with a total mechanical strain range of 2.0%).

5. Discussion and Outlook

As the modified-Langer-equation-based prediction for the number of LCF cycles to failure of about 870 is smaller by more than a factor of two than the about 1919 (HCF-related) full-length hot-run cycles to failure, obtained by the modified Goodman Equation (5), LCF

(at the suction side of the reference turbine blade) seems to be dominant in relation to the HCF failure (at the leading edge of the turbine blade). This LCF-over-HCF dominance of the fatigue life of the reference turbine blade is indirectly confirmed by the following sentence of [6]: "The requirement on LCF life was identified as the critical area for the blade material choice for this turbine".

However, the number of (HCF) cycles to failure of the uniaxial samples, used for fitting the parameters of the modified Goodman Equation (5), show two main drawbacks:

- This experimental data is (with HCF life values between 1 Mcycle to failure and 10 Mcycles to failure) several orders of magnitude smaller than the predicted HCF life of the reference turbine blade. A large uncertainty of the predicted HCF life of the reference turbine blade based on these HCF test results with uniaxial probes has to be assumed under these circumstances.
- The experimental HCF data is related to ambient temperature—whereas the hot-run temperature of the reference turbine blade is assumed to be 800 K.
- These two drawbacks will be eliminated in the near future at DLR Lampoldshausen by the following two measures:
- Additional HCF tests with Inconel 718 samples (under loading conditions, expected to result in the fatigue-life magnitude of the reference turbine blade).
- Elevated temperature correction of one or several of the parameters of the Goodman Equation (5).

Author Contributions: conceptualization, J.R.R.; methodology, J.R.R. and E.B.Z.; software, E.B.Z.; validation, J.R.R. and E.B.Z.; formal analysis, E.B.Z.; investigation, E.B.Z.; resources, J.R.R. and E.B.Z.; data curation, E.B.Z.; writing—original draft preparation, J.R.R.; writing—editing, J.R.R.; visualization, J.R.R. and E.B.Z.; supervision, J.R.R.; project administration, J.R.R.; DLR-internal funding acquisition, J.R.R. All authors have read and agreed to the published version of the manuscript.

Funding: The DLR-Institute of Space Propulsion in Lampoldshausen, Germany received DLR-internal funding for this research under the DLR project node number 8481293.

Data Availability Statement: Not applicable.

Acknowledgments: The authors of this paper would like thank Louis Souverein (ArianeGroup GmbH, Munich, Germany) for the exchanges on this topic within the framework of the Propulsion 2025 agreement between ArianeGroup and the space-propulsion-related DLR institutes.

Conflicts of Interest: The authors declare no conflict of interest. The funders had no role in the design of the study; in the collection, analyses, or interpretation of data; in the writing of the paper; or in the decision to publish the results.

References

1. Lee, H. *Space Shuttle Main Engine High Pressure Fuel Turbopump Turbine Blade Cracking*; NASA TM-100327; George, C., Ed.; Marshall Space Flight Center: Huntsville, AL, USA, 1988.
2. Nagao, N.; Nanri, H.; Okita, K.; Ishizu, Y.; Yabuki, S.; Kohno, S. The Modified Fuel Turbopump of 2nd stage engine for H3 launch vehicle. In Proceedings of the 7th European Conference for Aeronautics and Space Sciences (EUCASS), Milan, Italy, 3–6 July 2017. [CrossRef]
3. Holmedahl, K. Analysis and Testing of the Vulcain 2 Lox Turbine Blades for Prediction of High Cycle Fatigue Life. In Proceedings of the 36th AIAA/ASME/SAE/ASEE Joint Propulsion Conference and Exhibit, Huntsville, AL, USA, 16–19 July 2000; AIAA: Reston, VA, USA, 2012. [CrossRef]
4. Kalluri, S.; McGaw, M.A. Effect of Tensile Mean Stress on Fatigue Behavior of Single Crystal and Directionally Solidified Superalloys, NASA Technical Memorandum 103644. In Proceedings of the Symposium on Cyclic Deformation, Fracture, and Nondestructive Evaluation of Advanced Materials, San Antonio, TX, USA, 12–13 November 1990.
5. Saturday, E.G. Hot Section Components Life Usage Analyses for Industrial Gas Turbines. Ph.D. Thesis, Cranfield University, Cranfield, UK, 2015.
6. Trollheden, S.; Bergenlid, B.; Aglund, A.; Pettersson, A.I. Development of the Turbines for the Vulcain 2 Turbopumps. In Proceedings of the 35th AIAA/ASME/SAE/ASEE Joint Propulsion Conference & Exhibit, Los Angeles, CA, USA, 20–23 June 1999; AIAA: Reston, VA, USA, 2012. [CrossRef]

7. Ubulom, I. Influence of fluid-structure interaction modelling on the stress and fatigue life evaluation of a gas turbine blade. *J. Power Energy* **2021**, *235*, 1019–1038. [CrossRef]
8. Ansys. Available online: https://www.ansys.com/ (accessed on 1 September 2022).
9. Campello, D.; Tardif, N.; Baietto, M.-C.; Coret, M.; Desquines, J. Secondary creep behavior of Zr-4 claddings under LOCA conditions. In Proceedings of the Top Fuel 2016 Conference, Boise, ID, USA, 11–15 September 2016. Available online: https://hal.archives-ouvertes.fr/hal-01863188 (accessed on 24 December 2022).
10. Special Metals. INCONEL®Alloy 718. Available online: https://www.specialmetals.com/documents/technical-bulletins/inconel/inconel-alloy-718.pdf (accessed on 23 December 2022).
11. Caisso, P.; Barton, J.; Illig, M.; Margat, T. Development status of the Vulcain 2 engine. In Proceedings of the 36th AIAA/ASME/SAE/ASEE Joint Propulsion Conference and Exhibit, Las Vegas, NV, USA, 24–28 July 2000; AIAA: Reston, VA, USA. [CrossRef]
12. Macaluso, S.B. *Liquid Rocket Engine Turbines*; NASA SP-8110; NASA Lewis Research Center (Design Criteria Office): Cleveland, OH, USA, 1974.
13. Brown, A.M.; De Haye, M.; De Lessio, S. Application of Probabilistic Methods to Assess Risk due to Resonance in the Design of J-2X Rocket Engine Turbine Blades. In Proceedings of the 52nd AIAA/ASME/ASCE/AHS/ASC Structures, Structural Dynamics and Materials Conference, Denver, CO, USA, 4–7 April 2011; AIAA: Reston, VA, USA. [CrossRef]
14. Kitsche, W. *Operation of a Cryogenic Rocket Engine*; Springer Series in Aerospace Technology; Springer: Berlin/Heidelberg, Germany, 2011; ISBN 978-3-642-10564-7. [CrossRef]
15. Bruchhausen, M.; Fischer, B.; Ruiz, A.; González, S.; Hähner, P.; Soller, S. Impact of hydrogen on the high cycle fatigue behaviour of Inconel 718 in asymmetric push–pull mode at room temperature. *Int. J. Fatigue* **2015**, *70*, 137–145. [CrossRef]
16. Korth, G.E. *Effects of Various Parameters on the Fatigue Life of Alloy 718*; Superalloys 718, 625 and Various Derivatives; The Minerals, Metals & Materials Society: Warrendale, PA, USA, 1991.
17. VDM Metals. VDM®Alloy 718 (Nicrofer 5219 Nb), Material Data Sheet No. 4127, Revision 01. 2019. Available online: https://www.vdm-metals.com/fileadmin/user_upload/Downloads/Data_Sheets/Data_Sheet_VDM_Alloy_718.pdf (accessed on 23 December 2022).
18. Inconel 718 Technical Data. Available online: https://www.hightempmetals.com/techdata/hitempInconel718data.php (accessed on 23 December 2022).
19. Wahlén, U. The Aerodynamic Design of the Turbines for the Vulcain Rocket Engine. In Proceedings of the 31st AIAA/ASME/SAE/ASEE Joint Propulsion Conference and Exhibit, San Diego, CA, USA, 10–12 July 1995; AIAA: Reston, VA, USA, 2012. [CrossRef]
20. Bosson, R.; Sabin, P.; Turin, G. Improvements of the Hydrogen Turbopump for the Vulcain 2 Engine. In Proceedings of the 35th AIAA/ASME/SAE/ASEE Joint Propulsion Conference and Exhibit, Los Angeles, CA, USA, 20–24 June 1999; AIAA: Reston, VA, USA, 2012. [CrossRef]
21. Mårtensson, H.; Andersson, S.; Trollheden, S.; Brodin, S. Rocket Engines: Turbomachinery. In *Advances on Propulsion Technology for High-Speed Aircraft*; Educational Notes RTO-EN-AVT-150, Paper 5; RTO: Neuilly-sur-Seine, France; NATO Research and Technology Organization: Neuilly-sur-Seine, France, 2008; pp. 5-1–5-28. Available online: https://www.sto.nato.int/publications/STO%20Educational%20Notes/RTO-EN-AVT-150/EN-AVT-150-05.pdf (accessed on 24 December 2022).
22. Ellerbrock, H. VULCAIN 2: Thrust Chamber. ASTRIUM Space Transportation; Propulsion & Equipment. Available online: https://www.yumpu.com/en/document/view/17516895/vulcain-2-thrust-chamber-eads (accessed on 24 December 2022).
23. Riccius, J.R.; Zametaev, E.B.; Souverein, L.J. HCF, LCF and creep life analysis of a generic LRE turbine blade. In Proceedings of the AIAA SciTech Forum, San Diego, CA, USA, 3–7 January 2022; AIAA: Reston, VA, USA. [CrossRef]